FINAL TECHNICAL REPORT
SERDP SEED PROJECT # CU-1173
CONTRACT # DACA72-00-P-0056

SAR/GPR Matched Filter Processing for UXO Discrimination

December 21, 2001

Prepared by

Mirage Systems
1031 East Duane Avenue, Suite F
Sunnyvale, CA 94085-2626
Phone: (408) 524-7905
Fax: (408) 524-7903

i. Project Title

SAR/GPR Matched Filter Processing for UXO Discrimination

ii. Performing Organization

Mirage Systems
1031 East Duane Avenue, Suite F
Sunnyvale, CA 94085-2626
Phone: (408) 524-7905
Fax: (408) 524-7903
Principal Investigator: George J. Moussally
E-mail: gjmmirage@aol.com

iii. Project Background

This project addressed SERDP's need for technologies that can detect and discriminate unexploded ordnance (UXO), ranging in size from 20 mm shells to 2000 lb. bombs, from other items in the subsurface. The development of cost-effective detection and discrimination technologies is needed in the following three categories: (1) integrated systems that can cost-effectively survey large tracks of land, detect potential UXO, and discriminate UXO from clutter, (2) systems that are cued by other survey technologies that can cost-effectively and non-invasively interrogate the suspected item, and (3) processing technologies that can exploit the current state-of-the-art sensors to improve discrimination capabilities. This project addressed the above categories (1) and (3).

The project used an existing Ground Penetrating Radar (GPR) sensor to collect data from typical UXO targets (surface emplaced and buried). This sensor is a ground-mobile, standoff system (i.e., the GPR antenna is physically remote from the ground surface). The standoff nature of the sensor is significant in that it offers the potential for cost-effectively surveying large tracks of land. SAR techniques were used in the data collection and processing to form high-resolution 3D SAR images. Additionally, the data was processed using a matched-filter processing technique in order to achieve UXO target discrimination. The matched-filter processing technique aims to achieve target discrimination by exploiting target specific radar scattering features directly in the SAR image formation process.

iv. Objective

The project's objectives were to assess the degree of benefit achievable by using the standoff SAR/GPR to detect UXO and, additionally, to process the data with the matched-filter processing technique to achieve discrimination. More specifically, with regard to the matched-filter processing, we wished to determine the potential reduction in false positives achievable with this technique—the goal being to significantly reduce the occurrences of false positives typically encountered in the UXO cleanup process.

v. Technical Approach

The technical approach consisted of the following steps:

- Define a limited but reasonably diverse UXO target set intended to be representative of a wide range of UXO targets.
- For every UXO target in the set generate an appropriate matched filter by using the NEC-4 computer code to model radar scattering from that target.
- Simulate the anticipated performance to be achieved by the matched filters.
- Obtain inert UXO test targets for each target in the set.
- Collect SAR/GPR data under controlled conditions on the UXO test targets.
- Process the measured GPR data by using 3D SAR processing with and without the matched-filter processing.
- Assess performance by using the measured data to analyze the impact of the data collection and processing technique on reducing false positives.

vi. Summary

In general, the project results were mixed. On the plus side, the project demonstrated the utility of the GPR SAR sensor for <u>use in wide area UXO target detection</u>. Furthermore, the matched-filter processing was able to achieve some <u>discrimination benefit for UXO targets emplaced on the ground surface</u>. However, the matched-filter processing technique was <u>not effective for discriminating buried UXO targets</u>. It is believed that this limitation resulted from the simplifying assumptions underlying the scattering model used to generate the matched filters for the buried targets and the propagation model used to generate the SAR imagery. It is recommended that follow-on R&D activities focus on enhancing the mobility of the collection system, improving scattering and propagation models, and developing new UXO discrimination algorithms customized to exploit the novel data characteristics associated with a standoff GPR/SAR detection sensor.

vii. Results and Discussion

1. GPR Technology Description

a. Data Collection Sensor

The GPR data collection system is implemented on a towable trailer with a telescoping mast. Figure 1 is a photo of the system fielded at Yuma Proving Ground (YPG) with the telescoping mast fully extended (~14 m above ground). Located near the top of the mast (insert) and as shown in Figure 2 are a compact radar electronics unit (35 lbs., 19"x19"x7") and a split-V log-periodic antenna (150-1000 MHz). Above the GPR antenna is the mobile unit of a differential GPS positioning system. The radar electronics unit can operate from 20 MHz to 1200 MHz and provides a fully coherent signal reception capability. The radar uses a SW controllable, frequency domain waveform (i.e. FMCW linear chirp as opposed to an impulse) with switched hardware range gating to eliminate transmitter to receiver coupling and to allow direct ground bounce clutter to be range gated out. The end result is a high dynamic range UWB radar system with excellent sub-clutter visibility. A computer within the trailer functions as a radar controller to set the radar into various operating modes prior to data collection. During SAR operation this same computer serves to collect streaming radar data to disk via a high-speed data link from the radar electronics unit. Data is then transferred to a separate computer for further processing and for image generation. A functional block diagram of the data collection system is shown below in Figure 3 while Table 1 lists key radar parameters and their values.

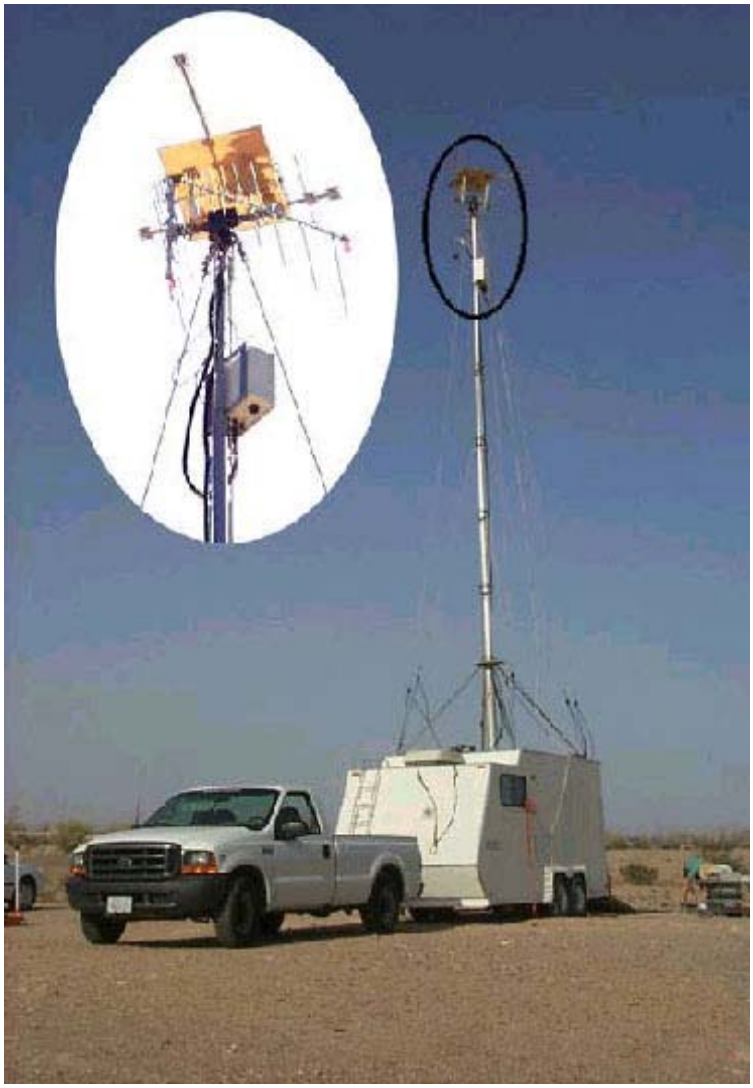

Figure 1 - Standoff GPR Data Collection System

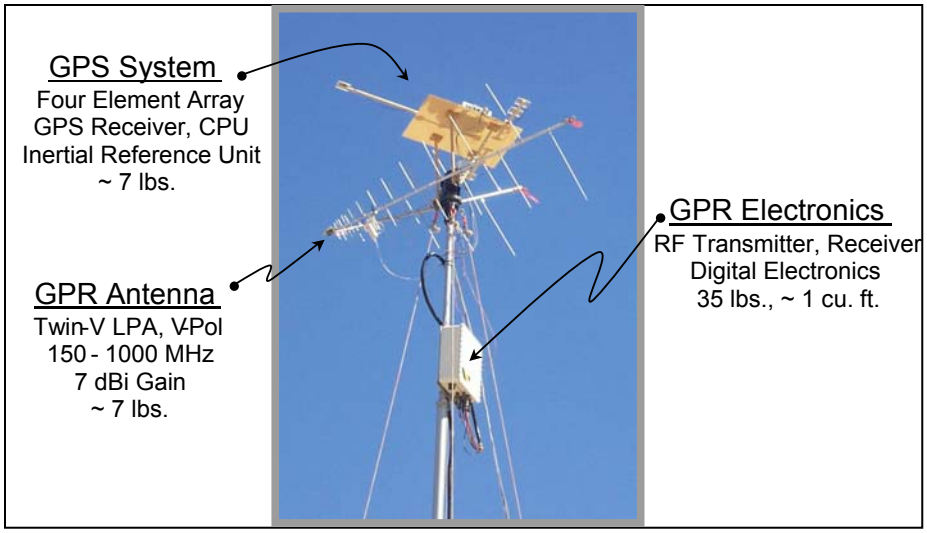

Figure 2 – Close-up of Mast Top

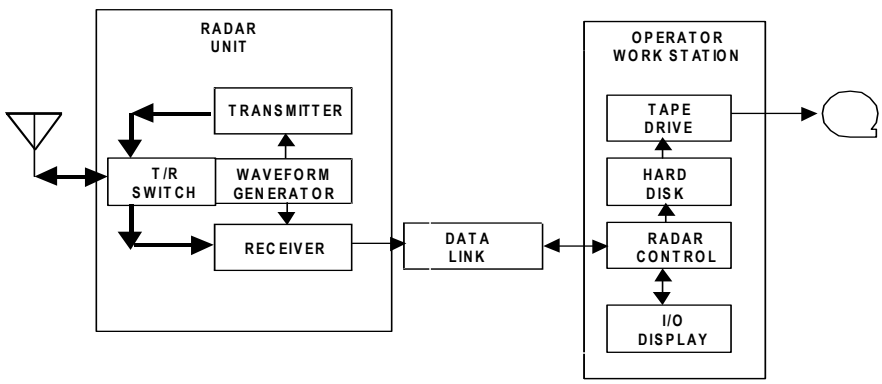

Figure 3 - Block Diagram of Data Collection System

Frequency Band	Ultra-Wide-Band, 20 MHz to 1200 MHz. Operating bandwidth is programmable with selective frequency notching capability.
Time-Bandwidth Product	75 dB.
Waveform	Swept FMCW (i.e. chirp), 30 chirps/sec. Each chirp is time gated (50% duty cycle). Parameters are SW programmable within constrained limits.
Radar Power Output	Adjustable to maximum of 10 w peak, 5-w average.
Receiver	High dynamic range, fully coherent, super-heterodyne.
Radar Data Output	16 bits I (In-phase), 16 bits Q (Quadrature).
Antenna	Vertically polarized, Twin-V, Log Periodic Array. Gain -5 to +8 dBi.

Table 1 – Key Radar Parameters

In order to achieve focused SAR images it is necessary to have accurate knowledge of the radar antenna position during its motion over the synthetic aperture. This position information is used to ensure proper focusing of the SAR image by phase compensating the data collected over the entire SAR path. This process is known as motion compensation and requires precise measurement of the position of the phase center of the GPR antenna.

The positioning measurement system utilized on this project used electronic repeaters that act as reference targets within the SAR field of view. Three repeaters are needed to provide an unambiguous 3D measurement of position. The repeaters, deployed on the ground within the survey region are compact (~ 15 cm high) and battery powered. A photo of a repeater is shown in Figure 4.

The repeater-based measurement technique works as follows. Each repeater receives the radar signal, alters it by imposing a pseudo-Doppler modulation onto the signal, and then transmits this modulated signal back to the radar. The repeater signals are, thus, embedded in the normal radar data stream; no special radar modifications are required to receive the repeater signals. A different Doppler frequency is used for each individual repeater allowing each repeater to be uniquely identified. After Doppler processing, the responses from the repeaters stand out above the background clutter with high signal quality (i.e., high signal to clutter ratio) because the repeater signals have been Doppler shifted away from the zero-Doppler background clutter. Due to the high quality of the repeater signals, with post processing of the data, the range between each repeater and the SAR antenna is precisely determined. A tri-lateration algorithm is then used on three repeater ranges to accurately locate the SAR antenna's 3D position. Only the precise relative locations of the repeaters with respect to each other are needed in order to form a sharply focused SAR image; absolute geo-location of the repeaters also allows the focused SAR image to be accurately geo-referenced as well. This system accurately positions the SAR antenna in 3D space to ~5 cm with a data update rate of ~30 Hz.

These physically small repeaters are battery-powered and the measurement technique requires no special radar modifications. Thus, the repeater technique achieves precise positioning needed for the SAR data at a high update rate with minimal additional hardware. The positioning measurement achieved in this manner allows high-accuracy motion compensation of highly dynamic SAR data to occur and, thus, provides for good focusing of the SAR image. On the other hand, this technique does require that multiple repeaters be deployed within the field-of-view of the radar. For applications where repeater deployment is impractical or otherwise undesirable, the differential Global Positioning System (dGPS) is used instead.

b. SAR Data Collection Geometry

Circular SAR Mode

Data was collected using a circular spotlight SAR mode, with the vehicle moving the radar sensor in an approximately circular path around the region to be surveyed. Figure 5 depicts a typical circular SAR geometry used to collect the data. The three reference repeaters used for the position measurement are shown depicted on the surface.

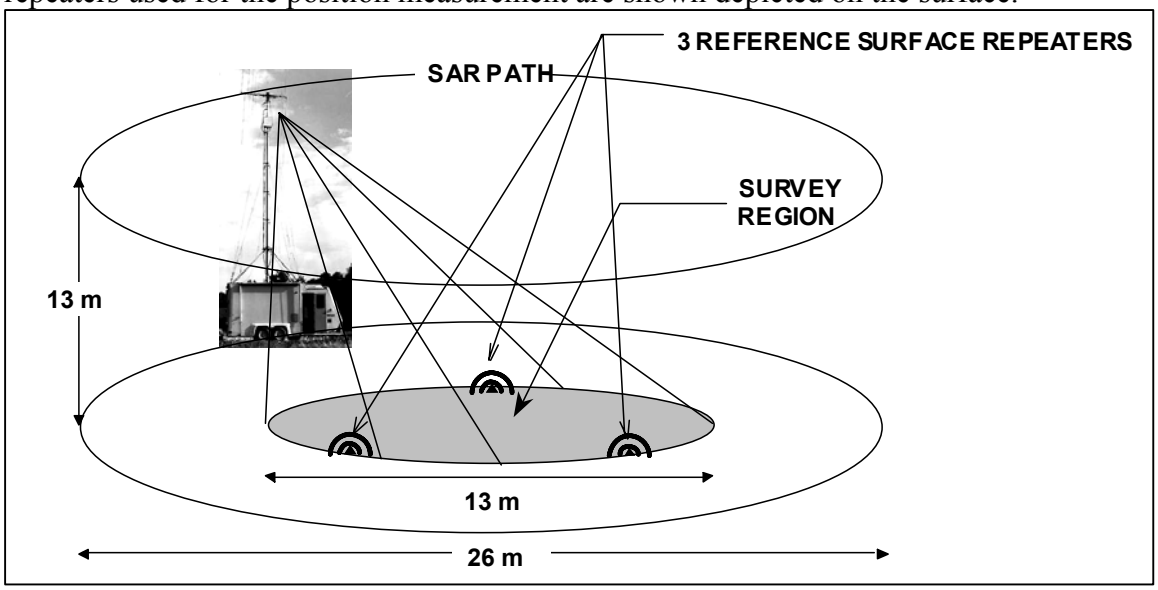

Figure 5 - Circular SAR Mode Geometry

With this geometry, the radar sensor views the survey region through a full 360-degrees maximizing the azimuthal angle diversity of the SAR data set. Radar data is collected over the entire circular SAR path, and that data is then subsequently processed, along with the repeater data, to form a 3D SAR image of the survey region.

Multiple Elevations

The system can collect data with the antenna at different heights above the ground. For this project, data was collected at three different antenna elevations above the ground surface. The elevations varied from 10 m and 13 m with the spacing between them being approximately equal. Figure 6 depicts the case of multiple elevation collection. With data collected in this fashion, the radar sensor views the survey region at multiple elevation angles further increasing the spatial angular diversity of the SAR data.

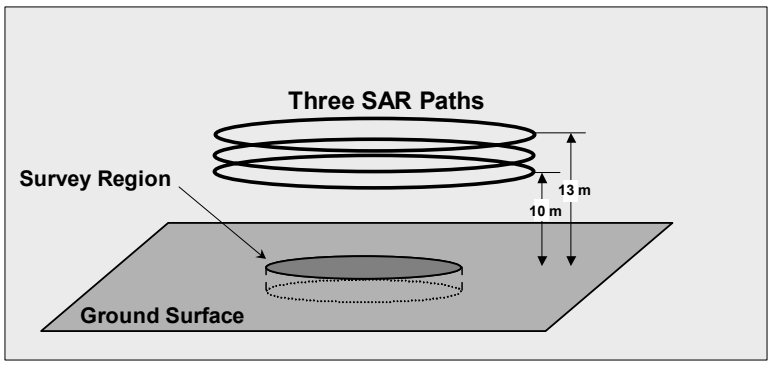

Figure 6 - Data Collection at Multiple Elevations

c. Data Processing Description

The data collected during the process was processed using two techniques: generalized 3D SAR imaging and matched filter processing. Generalized 3D SAR image processing makes no special assumptions about any targets being imaged. Effectively a simple point target scattering assumption is made, which is consistent with almost all SAR imaging processes. This imaging process is well suited for target location and detection but lacks a good capability to discriminate between targets of different types. With the matched filter processing technique, the point target scattering assumption is <u>not</u> made. Instead, the SAR image is formed by assuming that radar scattering being measured is due to a target of a specific size, shape, and composition. This technique is more useful for target discrimination. These two SAR imaging processes are described below.

Generalized 3D SAR Image Processing

A Fourier transformation of the radar data (as is commonly done in SAR image formation) is not particularly well suited for forming accurate SAR images of buried targets when using ground-based GPR. This poor suitability is due to several reasons, which violate assumptions that are inherent to forming SAR imagery via Fourier transformation. These reasons are:

- The data collection geometry is such that targets are not in the far-field of the SAR aperture.
- Practical constraints on the mobility of the sensor result in non-linear spatial sampling of the radar data.
- The radar ⇔ target phase propagation path is non-linear in k-space due to the existence of the in-ground path. This non-linearity results from the refraction of radar energy as it passes between the air-ground interface as well as the frequency dependency of the dielectric constant and/or the conductivity of typical ground soil at GPR frequencies.

These factors preclude the use of a simple Fourier transformation of the data to form accurate SAR images. Instead, the SAR imaging algorithm used in this application is based on the generalized SAR imaging approach of Mensa[1], with an extension to allow relevant ground electromagnetic characteristics (i.e., dielectric constant and conductivity) to be included within the SAR imaging process itself. With this approach, the sensor data over the entire SAR path and frequency range is numerically integrated to generate the SAR image. Specifically, the complex SAR image function, $\widetilde{I}$, is calculated as follows:

$$\widetilde{I}(\vec{r}_{VOX}, \widetilde{n}) = \sum_{\vec{r}_{RAD}} \sum_{f} \left\{ \widetilde{G}(f, \vec{r}_{RAD}) \widetilde{\Phi}^{*}(f, \vec{r}_{RAD}, \vec{r}_{VOX}, \widetilde{n}) \right\}$$

where $\widetilde{G}$ is the measured complex (i.e. I/Q) radar data.

$f, \vec{r}_{RAD}$ are the two radar measurement variables - frequency and radar position vector.

[1] Mensa, D.L., *High Resolution Radar Imaging.* Dedham, MA; Artech House, 1961.

$\tilde{\Phi}$ is the modeled complex propagation function from the radar to a buried voxel[2] and back to the radar.

$\tilde{\Phi}^*$ is the complex conjugate of $\tilde{\Phi}$.

$\vec{r}_{VOX}$ is the position vector of the voxel being imaged.

$\tilde{n}$ is the complex index of refraction for the ground, which incorporates the soil's dielectric constant and conductivity.

Note that the SAR image function depends upon $\tilde{n}$, which is obtained through modeling or measurements of ground characteristics. The SAR image generated using this technique can used to declare detections of potential targets of interest. Target detection is determined by simple thresholding of the image function's amplitude. The threshold level is established at some fixed level above the average background clutter measured in the SAR image of the total survey region.

Matched Filter Processing

With the matched filter processing technique, the basic concept is to achieve a discrimination capability by using target-specific radar scattering in the actual formation of the SAR imagery. With this approach the SAR image is formed by assuming that the radar scattering being measured from a particular volume is actually due to a particular type of target of a specific size, shape, and composition. Target scattering is modeled by using an electromagnetic scattering model to generate radar scattering from a particular target at GPR frequencies. This scattering model is then substituted for the simple point scattering model inherent conventional SAR imaging. A comparison is then made between the energy in this matched-filter SAR image with the energy in the conventional point scattering SAR image. If the matched filter SAR image yields significantly higher energy than the point scatter SAR image, then a target can be discriminated as being of the type that was modeled in the matched filter process. The image equation used for the matched filter imaging is similar to the basic imaging equation above

$$\tilde{I}(\vec{r}_{VOX}, \tilde{n}, m) = \sum_{\vec{r}_{RAD}} \sum_{f} \left\{ \tilde{G}(f, \vec{r}_{RAD}) \tilde{\Phi}^*(f, \vec{r}_{RAD}, \vec{r}_{VOX}, \tilde{n}, m) \right\}$$

where all parameters are the same as the previous basic imaging equation but with the addition of the parameter, m, which is a matched filter target index to identify the specific target used in modeling the propagation function, Φ.

[2] Voxel is an acronym for volume element. It is the 3D equivalent of a 2D pixel or picture element.

2. *Modeling*

a. UXO Target Set

The target set used in the project consisted of a variety of inert UXO ordnance targets recovered from UXO sites that had been cleaned up by the Army. The photo and table shown below in Figure 7 describe these targets.

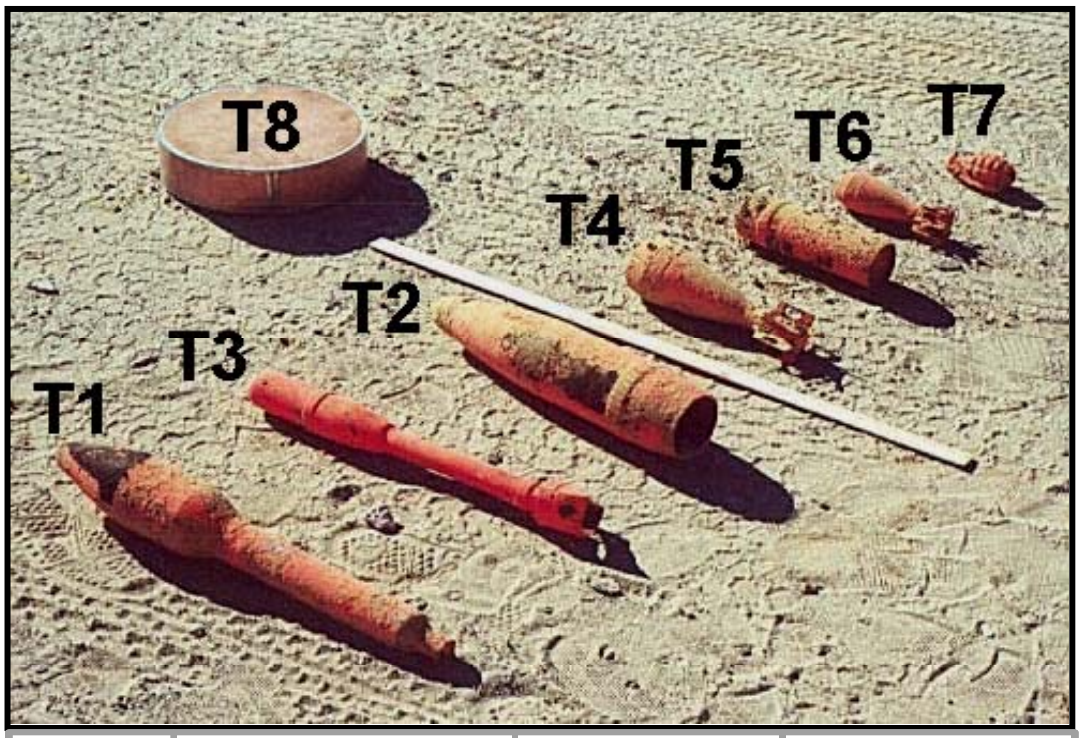

Type	Nomenclature	Length (inches)	Max Diam. (inches)
T1	3.5" Rocket	21.5	3.5
T2	105 mm Projectile	17.0	4.1
T3	2.36" Rocket	19.5	2.4
T4	81 mm Mortar	10.5	3.2
T5	75 mm Projectile	9.0	3.0
T6	60 mm Mortar	7.5	2.4
T7	MK II Grenade	4.5	2.0
T8	Metal Cylinder	12.0 Diam	3.0 Height

Figure 7 - Description of UXO Target Set

b. NEC Modeling of UXO Targets

For generating the matched filters on the project, we utilized the NEC4 electromagnetic (EM) scattering code, which is a computer that can analyze the scattering response of antennas of targets that are illuminated by EM energy. The NEC4 model code is based upon the numerical solution of integral equations by the method of moments and is supported and maintained by Lawrence Livermore National Laboratory[3]. One of the basic capabilities of this code is to calculate the complex (amplitude & phase) scattering cross section of targets that are defined by an input model. In addition, the code has the capability to determine scattering signatures for targets embedded in a dielectric medium and for targets buried under the ground. Although the NEC4 code allows for modeling target by both flat plates and wires, the modeling of targets under the ground makes use of the Sommerfeld-integral equations, which requires that the targets be modeled only using wire segments. NEC4 has been used and validated extensively by the EM modeling community and is generally considered to be the gold standard of EM scattering codes.

Target modeling guidelines, as identified in the NEC4 User's Guide, were followed during the modeling of the UXO targets shown in Figure 7 above. Specifically, the maximum length of a wire segment was designed to be less than 10% of the shortest radar wavelength, λ. Similarly, the wire radius, a, was selected such that $2\pi a/\lambda$ was much less than 1. As the target model becomes more detailed (*i.e.*, shorter, smaller wire segments) the processing time required to calculate the target radar cross section increases. Therefore, a compromise was made between the number of wire segments and processing time. For this study, the minimum wavelength was selected as 0.3m. Therefore, wire segments were made less than 3 centimeters and, for all targets modeled, the radius of the wire segments was set to 0.05 centimeters.

The targets of Figure 7 above were physically modeled as shown below in Figure 8 (a-h). This figure shows the wire frame target models generated via CAD software for use with the NEC4 modeling code. The AutoCAD DXF files generated by the CAD software were converted into NEC4 compatible wire frame input models by custom software.

[3] G. J. Burke, "Numerical Electromagnetic Code – NEC-4 Method of Moments Part I: User's Manual (NEC-4.1)", Lawrence Livermore National Laboratory, January 1992

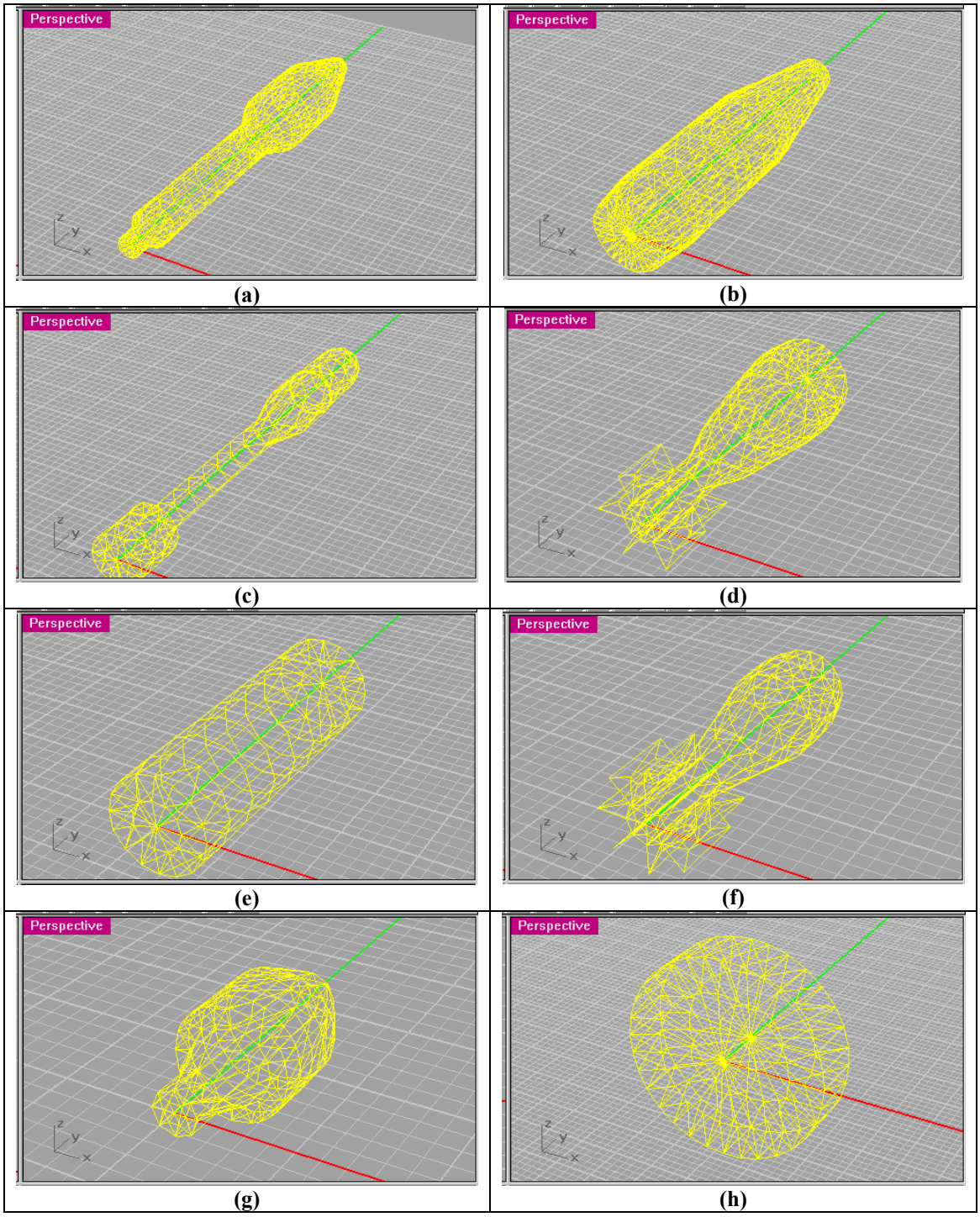

Figure 8 - Wire Frame Target Models Used to Generate RCS via NEC-4

Figure 9 shows an example output of the NEC-4 modeling code. For this example, target T2 (105mm artillery shell) was modeled vertically oriented as shown in Figure 9(a). The target was modeled in free space at a 24 degree incidence and in a dielectric medium of e=3.0 + j0.0 at an incidence angle of 45 degrees. The incidence angles were selected such that the incidence angle on the target in the dielectric would equal the incidence angle on the target in free space (*i.e.*, $\sin(45°)/\sqrt{\varepsilon} = \sin(24°)$) and hence the radar cross section as a function of frequency would vary only due to the difference in dielectric. As can be seen from Figure 9(b), the radar cross section of target in the dielectric medium (the blue curve) is compressed in frequency and attenuated in amplitude, as expected, as compared to the target in free space (the pink curve). Also, the failure of the model at high frequencies for the target embedded in the dielectric is evidenced by the noisy radar cross section response at high frequencies. This occurs since the target wire frame model no longer meets the criteria of node spacing being less than one tenth of a wavelength.

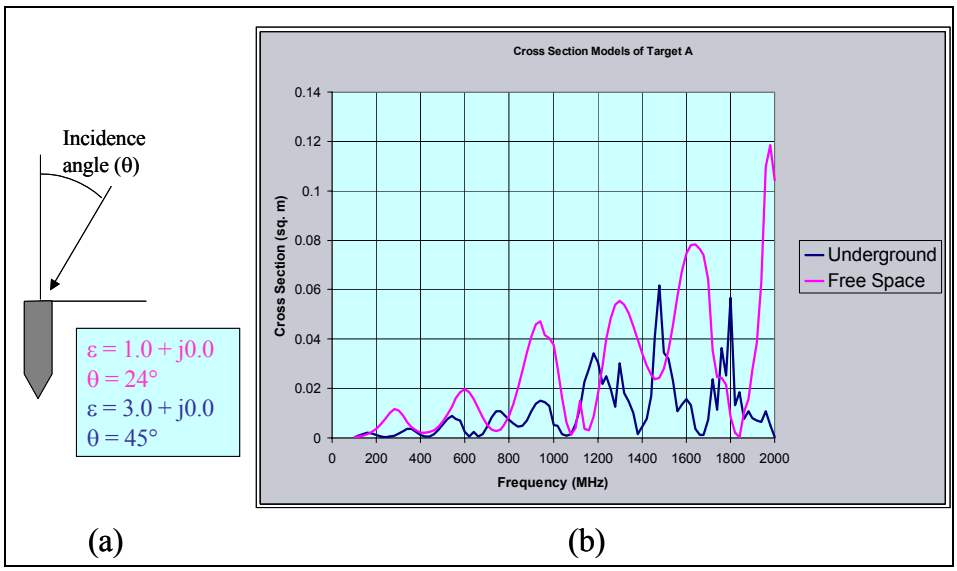

Figure 9 - NEC4 Modeling Example for Target T2 in Free Space and in a Dielectric of e=3.0+j0.0

The NEC4 code is very computationally intensive. Target models with many wire segments may require hours to determine the electromagnetic solution for the wire frame model at each frequency. Therefore, generating target models as a function of frequency, elevation angle, and azimuth angle can take several days per model depending upon the sampling in each dimension. Radar cross section models for several of the target shown in Figure 8 where generated using the NEC4 program as a function of frequency and then, for high frequencies, as a function of azimuth and elevation.

Figure 10 shows target T1, oriented horizontally, modeled above ground and 0.5 meters below the ground as a function of azimuth angle at 1000 MHz and a 50° elevation angle. Figure 11 illustrates target T1, oriented vertically, modeled 0.5 meters below the ground as a function of elevation angle at 1000 MHz (in this orientation, the target is independent of azimuth). Finally, Figure 12 shows target T1, oriented horizontally, modeled 0.5 meters below the ground as a function of frequency at 0° azimuth and 50° elevation.

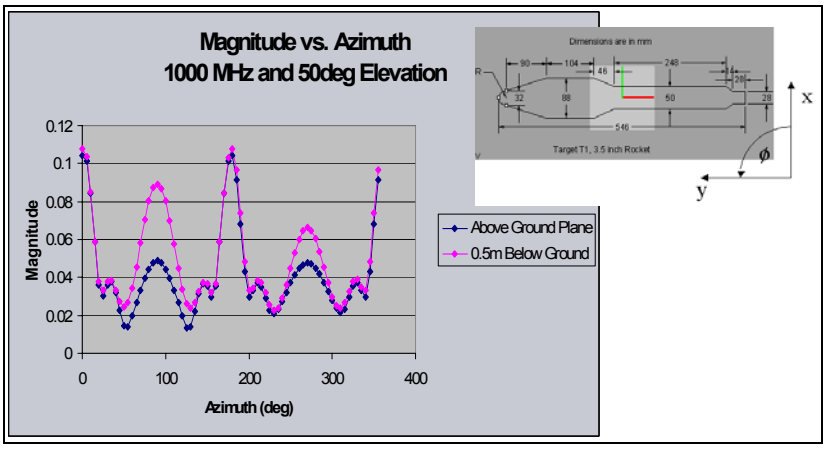

Figure 10 - NEC4 Modeling Results for Target T1 as a function of Azimuth Angle at 1000 MHz and 50° Incident Elevation Angle

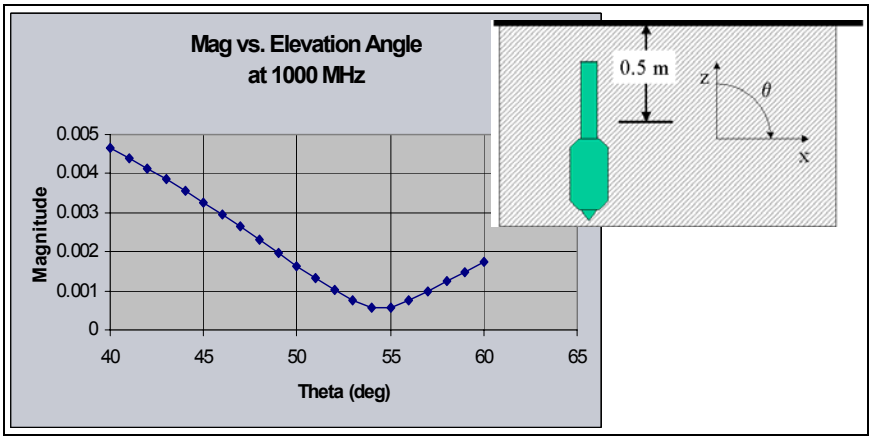

Figure 11 - NEC4 Modeling Results for Target T1 as a function of Elevation Angle at 1000 MHz

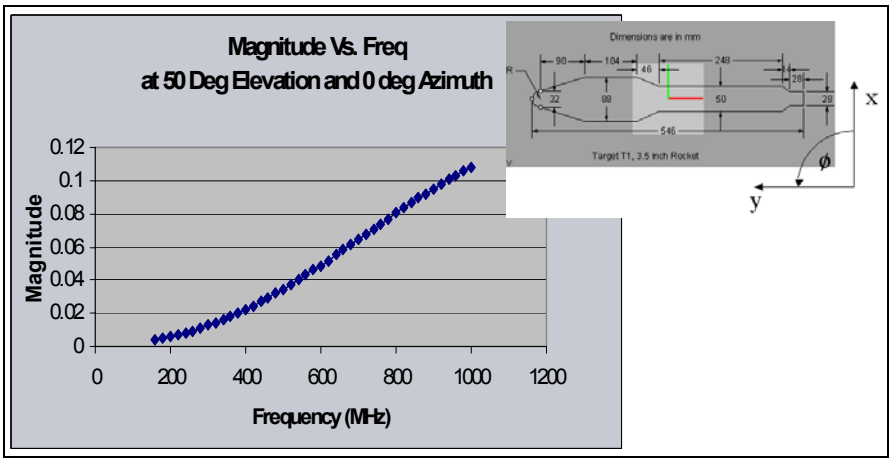

Figure 12 - NEC4 Modeling Results for Target T1 as a function of Frequency at 0° Incident Azimuth Angle and 50° Incident Elevation Angle

Results from these studies identified the appropriate frequency and spatial angle spacing for target model generation. The radar cross section for all target models shown in Figure 8 were calculated at the following frequency and spatial angle values:

Table 2 – Sampling Parameters for Matched Filter Calculations

	Start	Stop	Increment
Frequency	100 MHz	1100 MHz	200 MHz
Azimuth	0°	360°	10°
Elevation	40°	60°	5°

Thus, there were a total of 6 frequency samples with 5 elevation samples at each frequency and 37 azimuth samples at each elevation. Additionally, each target was modeled at three orientations: vertical, horizontal, and slanted at 45° relative to vertical.

c. Matched Filter Simulation

In order to estimate the potential benefit of using the matched filters in the GPR processing prior to data collection, a computer analysis was performed on simulated target data. As a first step, potential processing gains achieved by using known target radar cross sections can be estimated as the normalized coherent sum over frequency of the target scattering times the conjugate of the scattering of the matched filter model. That is,

$$I_{m,t} = \frac{\left| \sum_f \sigma_t(f) \cdot \sigma_m^*(f) \right|}{\left| \sum_f \sigma_m(f) \right|}$$

where $\sigma_t(f)$ is the target scattering as a function of frequency, f

$\sigma_m(f)$ is the scattering of the matched filter model as a function of frequency, f

$I_{m,t}$ is the approximate processing gain achieved for target t using model m

Synthetic analysis was performed using three target models, target T2, a 105mm artillery shell, target T5, a 75mm mortar, and target T6, a 60mm projectile. Table 3 illustrates the approximate gains achieved by utilizing target signatures as determined by the above equation. These processing gains represent the increase over the gains achieved without using a target model (i.e., by processing with a point source response). Table 3 illustrates that significant target gains above the point source response can be achieved by using target models that approximate the actual target present. For example, the T5 and T6 matched filters both yield similar processing gains (9.6 dB and 9.2 dB) when processed using scattering data from target T5. This is understandable considering the fact that T5 and T6 are similarly sized and shaped.

Table 3 - Approximate Processing Gains Expected by Using Target Radar Cross Section Information During GPR Processing

		Target		
		Target T2	Target T5	Target T6
Assumed Matched Filter	Target T2	17.6 dB	16.6 dB	-11.8 dB
	Target T5	14.2 dB	19.2 dB	-.4 dB
	Target T6	4.4 dB	18.4 dB	15.6dB
	Point Target	0.0 dB	0.0 dB	0.0 dB

In order to further assess the potential processing gain achieved by using target radar cross section information in the GPR synthetic aperture radar processing, buried target data was simulated using the NEC4 modeling code. Specifically, GPR data sets were simulated for vertically oriented targets buried at the center of a pit. Figure 13 shows the geometry used for computing the simulated data.

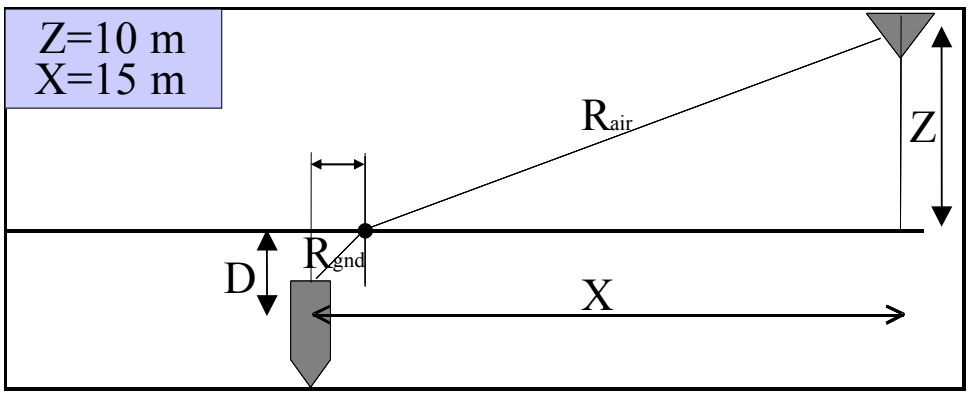

Figure 14 – Geometry Used For Matched Filter Calculations

Using this geometry and ground parameters, the phase of the simulated radar data was calculated by first selecting a target location (0 m on the X-axis, 0 m on the Y-axis, -0.5 m on the Z-axis), then determining the path length (phase) to the target as a function of position and frequency, and finally multiplying the phase due to path length by the target radar cross section. (Note, although current GPR processing does not utilize amplitude information, simulated data was generated by path phases and the radar cross section of the model targets.) Specifically, path lengths are calculated as follows:

$$R_{air} = \sqrt{Z^2 + (X - dX)^2}$$

$$R_{gnd} = \sqrt{D^2 + dX^2}$$

where $dX \approx \dfrac{X \cdot D}{D \cdot e^{-(n'-1)^2} + \sqrt{(n'^2 - 1) \cdot X^2 + n'^2 \cdot Z^2}}$

Then, the resultant radar response as a function of frequency and position is determined by the phase change calculated as:

$$\Delta\psi = 2 \cdot k \cdot (R_{air} + n' R_{gnd}) + \angle\{\, \sigma_T(\theta, \phi, f) \,\}$$

where: n' is the real component of the refractive index

$k = 2\pi / \lambda$

and $\angle\{\, \sigma_T(\theta, \phi, f) \,\}$ is target scattering phase as a function of position and frequency.

Synthetic data was generated for targets T2, T5, and T6 buried at the center of the imaging area at a depth of 0.5 m. Each synthetic target data set was processed with the GPR imaging code without a target model, and with target models corresponding to targets T2, T5, and T6. The volume imaged was –1 m < x < +1 m, -1 m < y < +1 m, and –0.5 m < z < 0.0 m. Figure 14 shows and iso-surface representation of processing the synthetic data for target T2 with the four target models (point source, T2, T5, and T6).

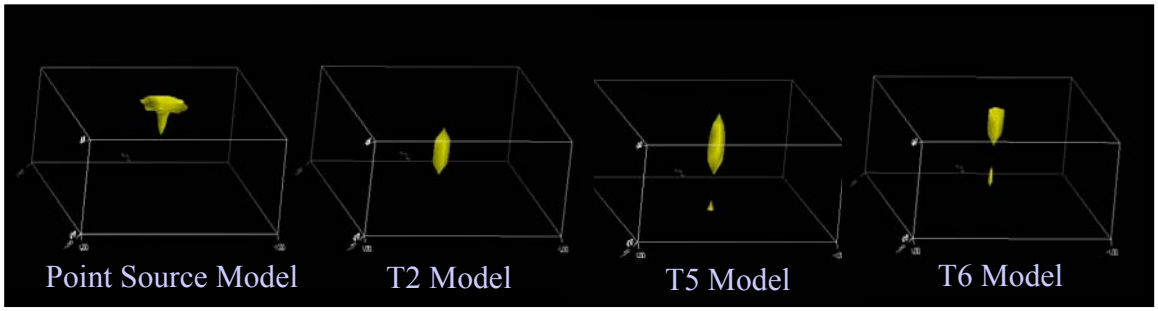

Figure 15 - Synthetic results for Target T2

As can be seen from Figure 14, using a target T2 model on synthetic target T2 data provides the best localization of the target and the least amount of residual clutter, as expected. More interesting is the result of processing target T2 with a point source model. In this case, the target response appears to be clustered at the surface, z = 0 m, and is not localized. Similarly, processing T2 data with the T6 model results in a similar scenario where most of the focused target energy occurs near the surface. However, using the target T5 model provides similar results to the target T2 model. These results agree with the approximations given by the coherent sums over frequency presented in Table 3. To illustrate further, Figures 15(a) and (b) show volume slices of the target T2 iso-surfaces shown in Figure 14 at z = -0.1 meter and z = -0.5 meters, respectively.

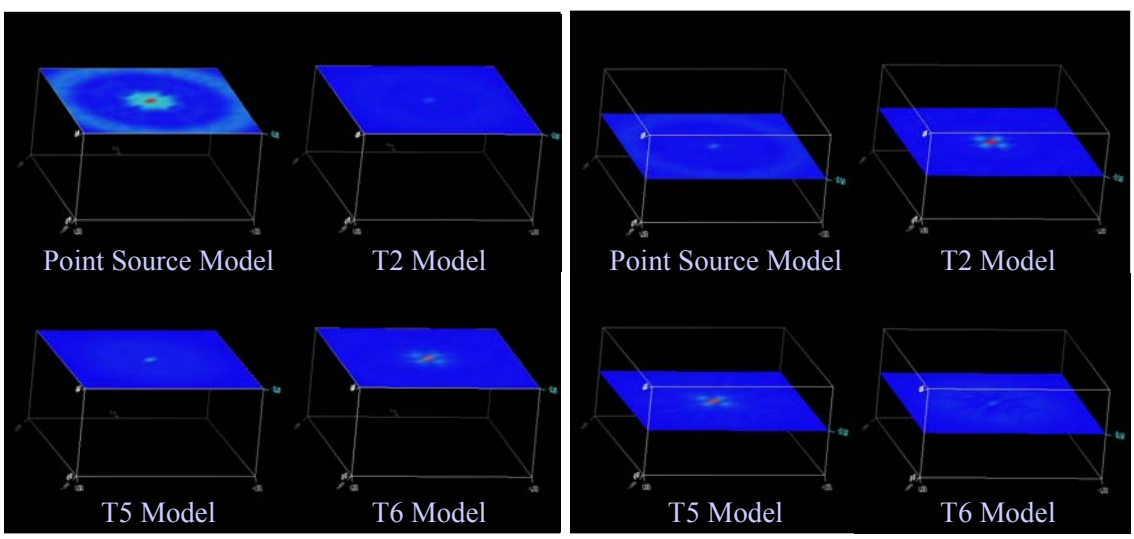

(a) (b)

Figure 16 - Elevation Cuts at (a) z = 0.1 m and (b) z = 0.5 m for T2 Synthetic Data Processed with Four Different Matched Filter Models

Figure 16 shows similar results for target T6. As with target T2, the best performance (least amount of residual clutter and best target localization) occurs when we process the synthetic data with the appropriate target model. Also, as with target T2, the use of a point source model results in target energy occurring at the surface and widely distributed spatially. Finally, by using the T2 or the T5 model, processed results are similar to those generated with the T6 model however, the target response is less localized and exhibits lower signal to noise. To illustrate further, Figures 17 (a) and (b) show volume slices of the target T6 iso-surfaces shown in Figure 16 at z = -0.1 m and z = -0.5 m, respectively.

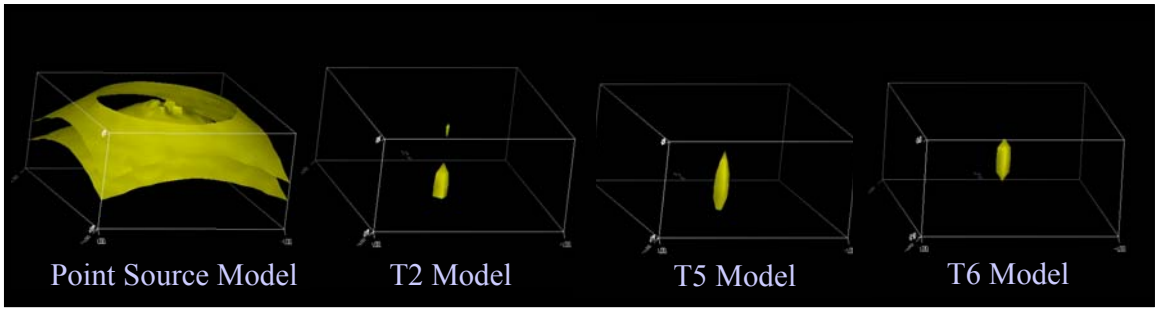

Figure 17 - Synthetic Results for Target T6

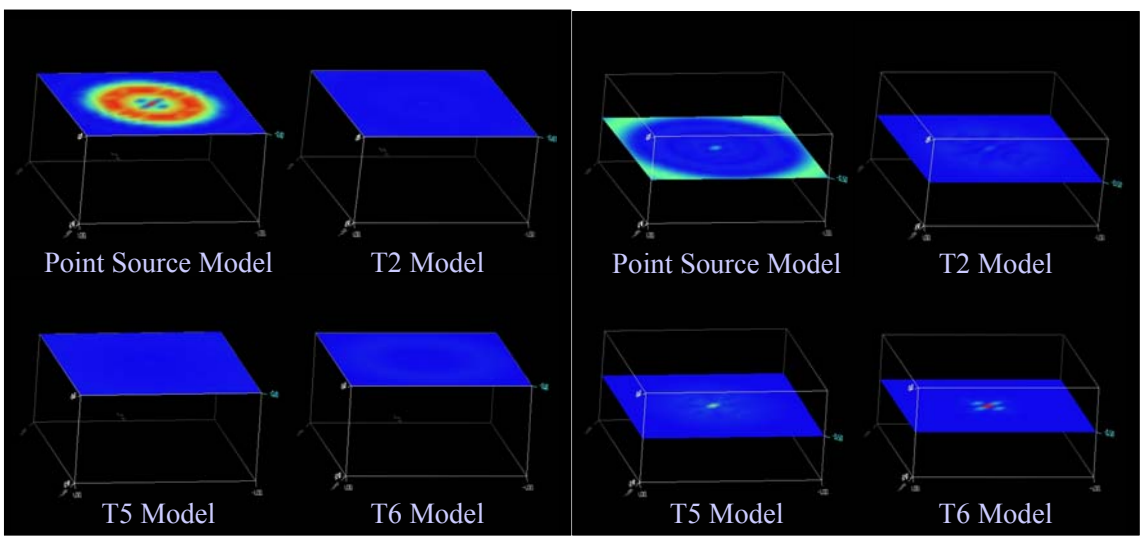

(a) (b)

Figure 18 - Elevation Cuts at (a) z = -0.1 m and (b) z = -0.5 m for T6 Synthetic Data Processed with Four Different Matched Filter Models

3. *Test Description*

During the course of the project GPR testing occurred at the US Army's Yuma Proving Ground (YPG) in Yuma AZ. The test site and test conditions are described below.

a. Test Site

Testing occurred at YPG's Steel Crater UXO test site adjacent to the Phillips Air Drop Zone. Mr. Stephen Patane, YPG Test Director, provided logistical support during the tests and assisted during testing. Figure 18 depicts the Steel Crater UXO test site showing the specific region of the site used for the tests. This region (designated as Area of Target Burial in the figure) is adjacent to the northern boundary of Boom Road near the end of the roadway.

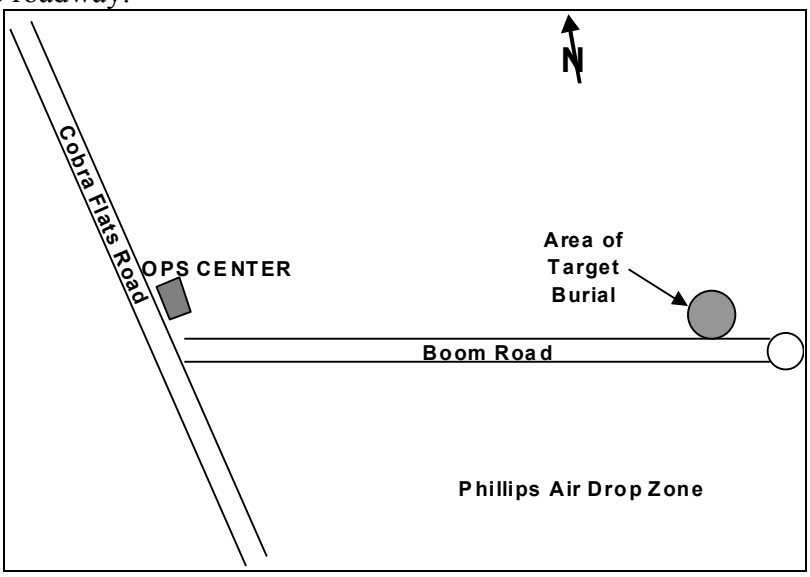

Figure 19 - Steel Crater UXO Test Site Used For Testing At Yuma Proving Grounds

Figure 19 is a photo of the area of target burial taken from Boom Road looking toward the northeast. The GPR data collection vehicle can be seen parked along the northern boundary of Boom Road. Targets were buried as indicated near the center of the circular region (dotted line) circumscribed by red traffic cones visible on the surface.

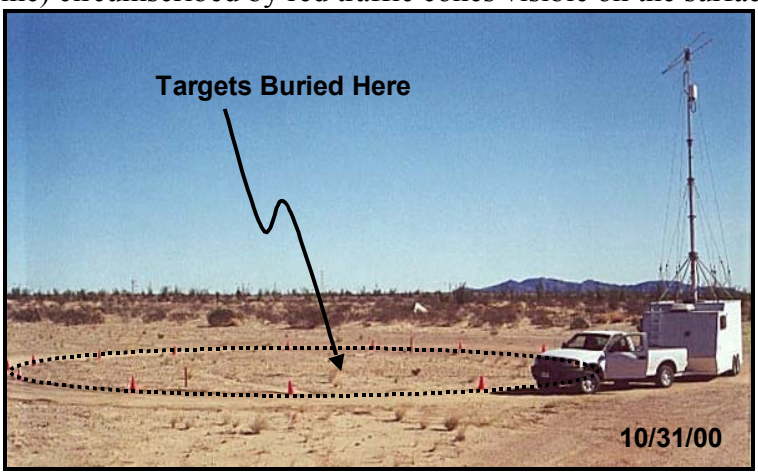

Figure 20 - Area of Target Burial

b. Test Conditions

The terrain in the immediate vicinity of the test site was generally flat and level as is apparent from the photo of Figure 19. Some small, sparse scrub vegetation is intermittently scattered throughout the area. Some of this vegetation is visible in the foreground of the photo. Generally this scrub vegetation is less than 2 feet in height. Soil conditions can generally be described as sandy soil with low water content. At the time of testing the soil was reasonably dry although a rainstorm had passed through the area ~10 days before tests began and some remnant moisture was evident in the top ~½ meter of soil. Measurements on the electromagnetic characteristics (i.e., dielectric constant and conductivity) of YPG soil samples collected in the general region of the Steel Crater site had been previously made by the USGS[4]. This data was used to determine a reasonable set of parameters for the ground model used in the SAR imaging process.

SAR Geometry

GPR data was collected in a circular spotlight SAR mode. With this mode, data is collected as the sensor vehicle is moved in an approximately circular path around the target region to be imaged. For each target condition, SAR data was collected at three equally spaced elevations of the GPR antenna between 10 m and 13 m. The effect of collecting data at multiple elevations is to increase the spatial angular diversity of the SAR data and added diversity in the data helps to reduce clutter. The geometry of the SAR data collection that was used is depicted in Figure 20.

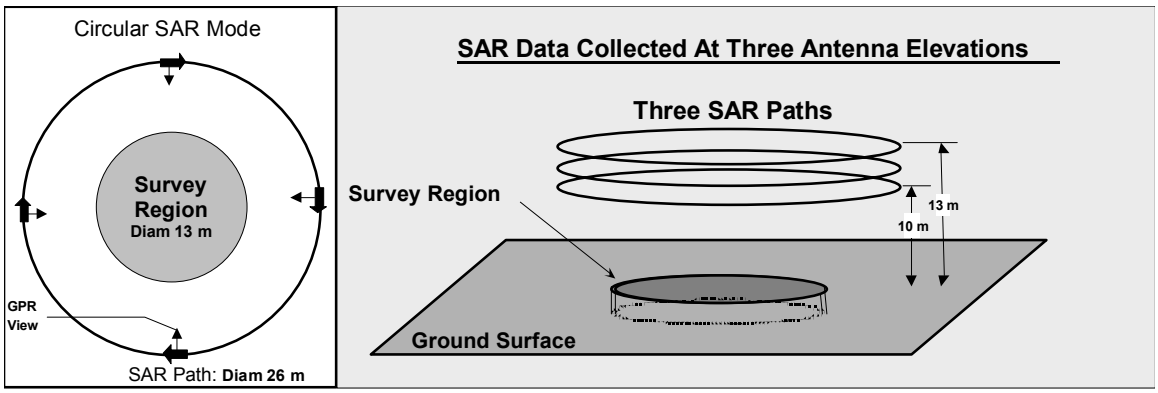

Figure 21 - Geometry of Circular SAR Data Collection

Target Conditions

Data was collected individually on each of the 8 targets (T1 – T8) previously characterized and described in Figure 7. For each target, SAR data was collected under 4 different test conditions: surface emplaced flat, buried with target axis vertically oriented, buried with target axis horizontally oriented, and buried with target axis tilted at 45°. Target axes are defined as the symmetry axes of the targets (all targets were considered to approximate bodies of revolution). Burial depths of the targets (measured from surface to

[4] Olhoeft, G. R. and Capron, D. E., "Laboratory Measurements of the Radiofrequency Electrical and Magnetic Properties of Soils from near Yuma, Arizona", Open File Report 93-701, U.S. Dept. of Interior, U.S. Geological Survey, 1993.

target center) ranged from 10 cm to 30 cm with largest targets being buried the deepest and the smallest targets being closest to the surface. For example, Figure 21 is a

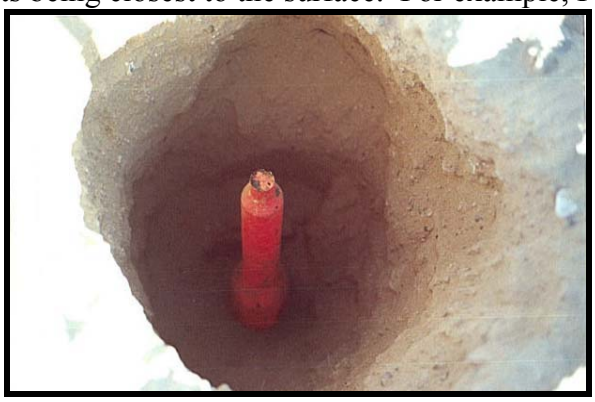

Figure 22 – Target T1 Being Buried

photo showing target T1, the 3.5" rocket, being buried vertically oriented with nose down. Burial depth was 30 cm below the surface as measured to target center. The photo was taken immediately before the excavated soil was used to backfill the hole. Additionally, for calibration and reference purposes, a number of SAR data collections were made without any targets (NONE) and with other reference targets (REF) placed on the surface. Table 4 below shows the matrix of test conditions under which SAR data collections occurred.

Table 4 – SAR Data Collection Test Matrix

Target	Orientations	Burial Depth	Ant. Elevations	# SAR Collections
NONE	NA	NA	Hi, Mid, Low	12
T1	flat	On Surface	Hi, Mid, Low	3
T1	H,V,T	30 cm	Hi, Mid, Low	9
T2	flat	On Surface	Hi, Mid, Low	3
T2	H,V,T	30 cm	Hi, Mid, Low	9
T3	flat	On Surface	Hi, Mid, Low	3
T3	H,V,T	30 cm	Hi, Mid, Low	9
T4	flat	On Surface	Hi, Mid, Low	3
T4	H,V,T	20 cm	Hi, Mid, Low	9
T5	flat	On Surface	Hi, Mid, Low	3
T5	H,V,T	20 cm	Hi, Mid, Low	9
T6	flat	On Surface	Hi, Mid, Low	3
T6	H,V,T	20 cm	Hi, Mid, Low	9
T7	flat	On Surface	Hi, Mid, Low	3
T7	H,V,T	10 cm	Hi, Mid, Low	9
T8	flat	On Surface	Hi, Mid, Low	3
T8	H,V,T	20 cm	Hi, Mid, Low	9
REF	flat	On Surface	Hi, Mid, Low	18
	H= Horizontal V = Vertical T = 45 deg tilt	Depth Is Surface to Target Center	Hi = 13 m Mid = 11.5 m Low= 10 m	126 Total SAR Collections

4. Test Results

The SAR data collected was initially processed to extract GPR antenna position information from the electronic reference repeaters. This information was then used to calculate the appropriate propagation function for use in the SAR imaging process. Use of the GPR antenna position in this manner essentially accomplishes the motion compensation needed to form focused SAR imagery.

When the position information was extracted several of the data sets appeared to have poor quality data coming from the electronic reference repeaters. Upon examination of the data collection log it was discovered that the repeater batteries had been changed immediately prior to the poor quality data sets. Additionally, data quality appeared to improve significantly when an additional set of batteries were used to replace this older set of batteries. The conclusion is that the poor quality data sets resulted from the use in the repeaters of an old battery set that had been left over from tests conducted during the previous year. As a result of this, a number of the SAR data sets collected were unable to be processed into SAR imagery because of the lack of adequate position data needed to accomplish the motion compensation. Table 5 below indicates which data sets had good enough quality position data for SAR imagery processing.

Table 5 – SAR Position Data Quality

Target Type	Burial Depth	Target Orientation	ANTENNA ELEVATION		
			LOW	MID	HIGH
T1	Surf	Flat	GOOD	GOOD	GOOD
T1	30	H	GOOD	GOOD	GOOD
T1	30	V	GOOD	GOOD	GOOD
T1	30	T	GOOD	GOOD	GOOD
T2	Surf	Flat	GOOD	GOOD	GOOD
T2	30	H	BAD	BAD	BAD
T2	30	V	BAD	BAD	BAD
T2	30	T	BAD	BAD	BAD
T3	Surf	Flat	GOOD	GOOD	GOOD
T3	30	H	BAD	BAD	BAD
T3	30	V	BAD	BAD	BAD
T3	30	T	BAD	BAD	BAD
T4	Surf	Flat	GOOD	GOOD	GOOD
T4	20	H	BAD	BAD	BAD
T4	20	V	BAD	BAD	BAD
T4	20	T	BAD	BAD	BAD
T5	Surf	Flat	GOOD	GOOD	GOOD
T5	20	H	GOOD	GOOD	GOOD
T5	20	V	BAD	BAD	BAD
T5	20	T	BAD	BAD	BAD
T6	Surf	Flat	GOOD	GOOD	GOOD
T6	20	H	GOOD	GOOD	GOOD
T6	20	V	GOOD	GOOD	GOOD
T6	20	T	GOOD	GOOD	GOOD
T7	Surf	Flat	GOOD	GOOD	GOOD
T7	10	H	GOOD	GOOD	GOOD
T7	10	V	GOOD	GOOD	GOOD
T7	10	T	GOOD	GOOD	GOOD
T8	Surf	Flat	GOOD	GOOD	GOOD
T8	20	H	GOOD	GOOD	GOOD
T8	20	V	GOOD	GOOD	GOOD
T8	20	T	GOOD	GOOD	GOOD

a. Example 3D SAR Imagery

Data sets with good quality position data were processed into 3D SAR imagery using the imaging process described in Section 1c. An example of a 3D SAR image (iso-surface view) depicting three reference repeaters is shown in Figure 22 along with a photo of the three repeaters sitting on the ground. The 3D volume depicted in the SAR image is 8 m x 8 m x 1 m (x,y,z) and the z scale shown in the SAR image varies from +0.2 m above the surface to -0.8 m below the surface. The three repeaters were arranged in an equilateral triangular arrangement.

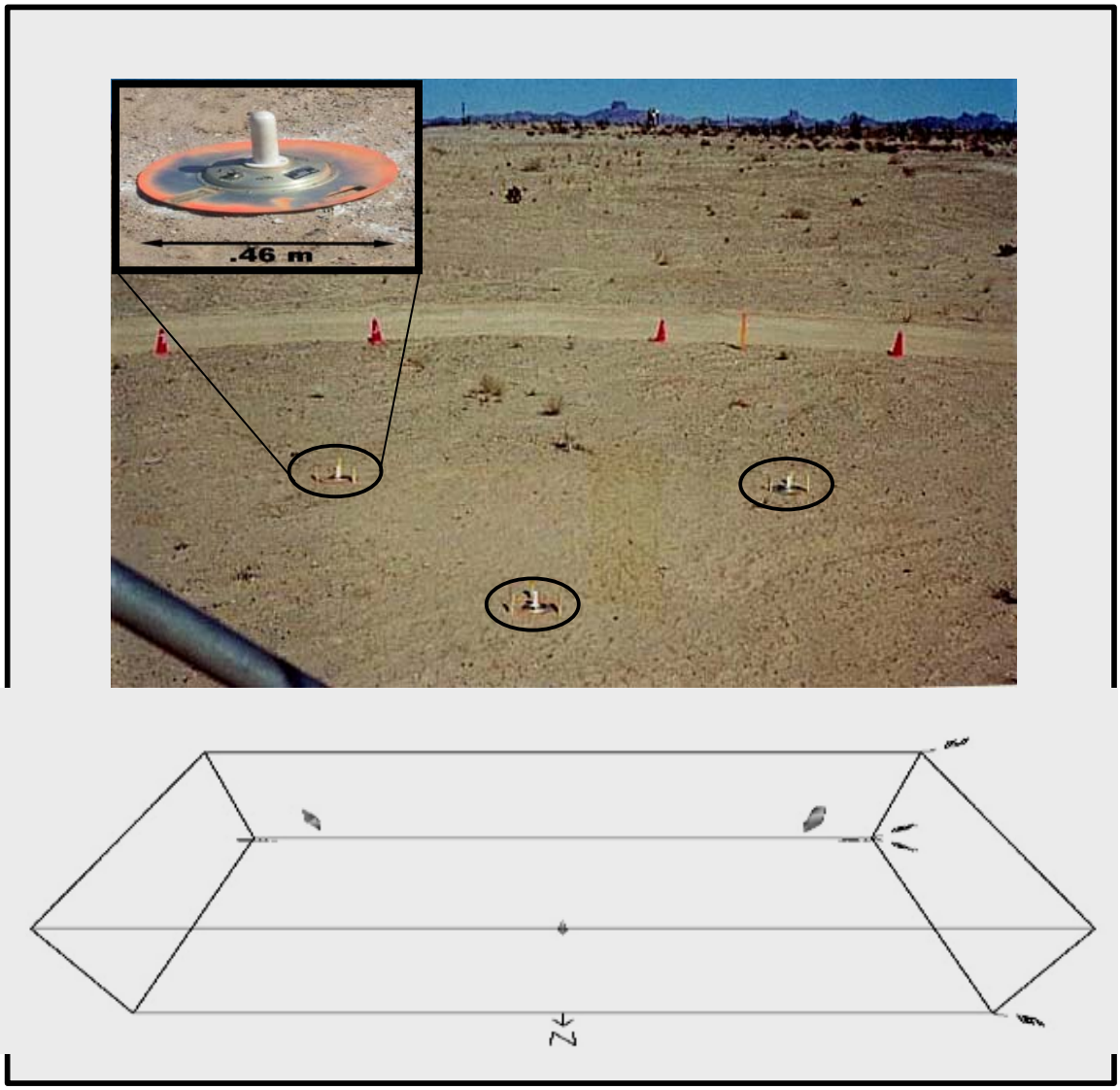

Figure 22 – Photo and 3D SAR Image of Three Surface Targets. SAR Image is an Iso-Surface View Showing a Volume of 8 m x 8 m x 1 m.

Figure23 shows three orthogonal sections views of the same SAR image with the front sectional view indicating that each repeater SAR image is within several centimeters of the ground surface (z = 0 m) where they were actually placed. The free-space spatial resolution of the SAR image in the x, y directions (SAR cross range) is ~14 cm. This depends upon the radar wavelength used and the SAR collection path geometry. In the z-direction (SAR down range) the nominal resolution is ~21 cm, which depends upon the radar's operating bandwidth (700 MHz in this case). The three repeaters are properly positioned in 3D in the SAR image to within a few centimeters.

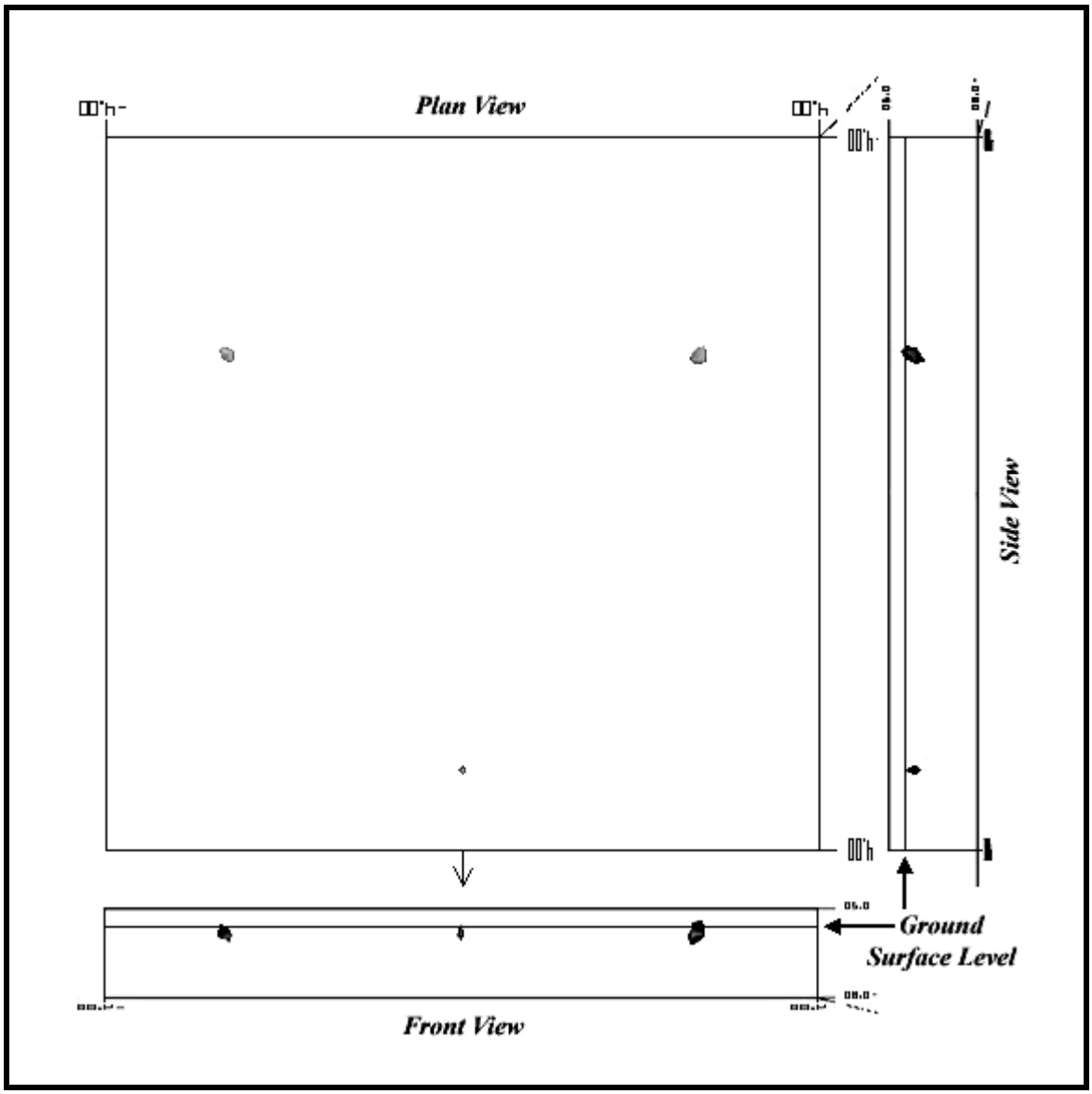

Figure 23 – Orthogonal Sectional Views of the 3D SAR image Shown in Figure 22.

Figure 24 is a 3D SAR image and orthogonal sectional views of target T8, the 12 inch diameter right circular cylinder, placed on the surface in the center of the image along with the three reference repeater targets. The size and scale of the 3D SAR image is the same as the images shown above. All targets are positioned within the SAR image to within a few centimeters.

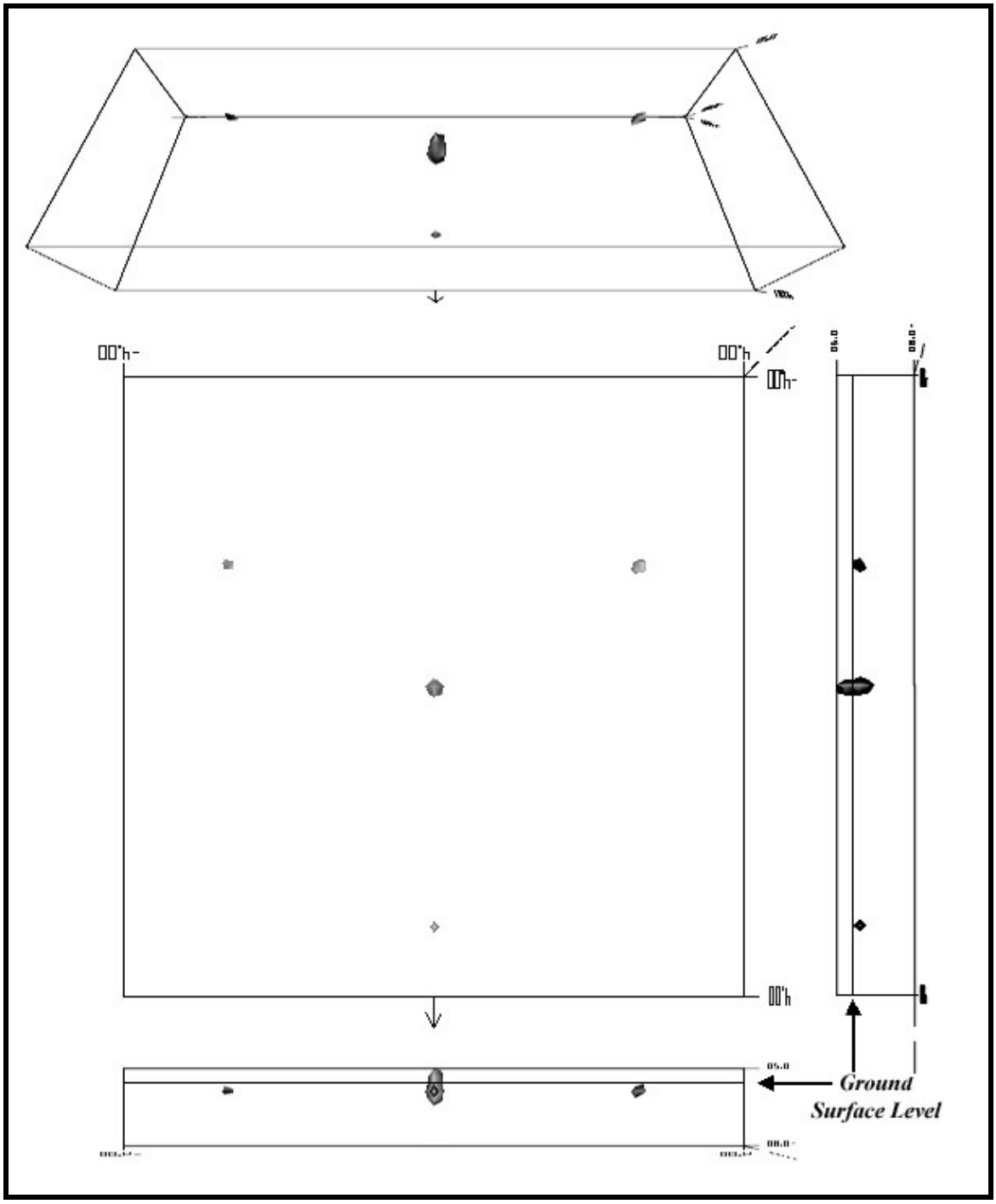

Figure 24 - 3D SAR Image of Three Reference Targets and Target T8, All On the Surface.

Figure 25 is a 3D SAR imageof target T8 similar to Figure 24 but in this case the target is buried 30 cm below the surface. The size and scale of the 3D SAR image are the same as the images shown above. Target T8 has been correctly imaged below the ground surface level and all of the targets are positioned within the SAR image to within a few centimeters.

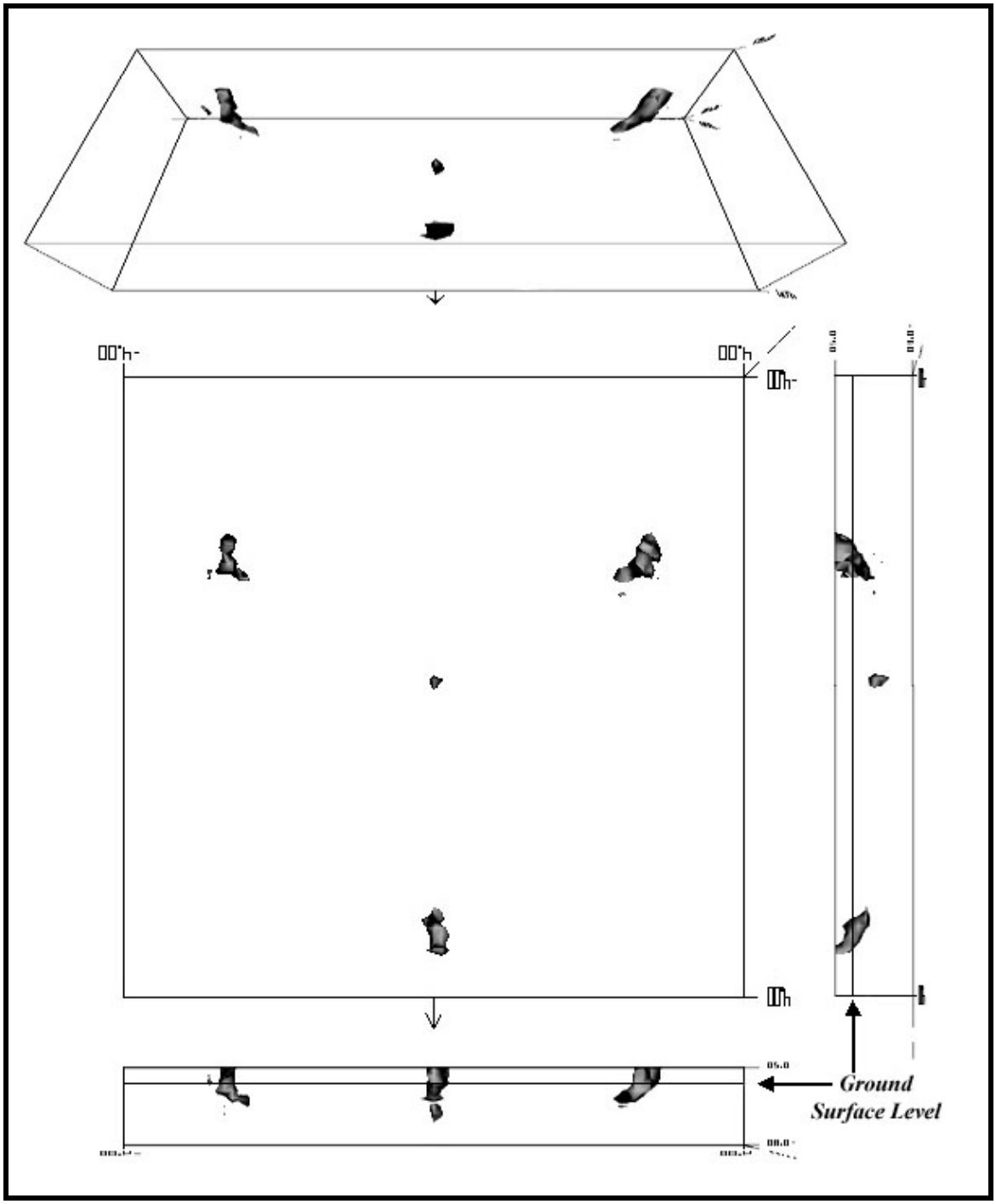

Figure 25 - 3D SAR Image of Three Reference Targets On the Surface and Target T8 In the Center of the Image and Buried 30 cm Below the Surface.

Figure 26 is a small region of the image in Figure 25 centered about the target T8. The volume in this image is 2 m x 2 m x 1 m. The ground truth of the target T8 is superimposed (in light grey) within the SAR sectional views.

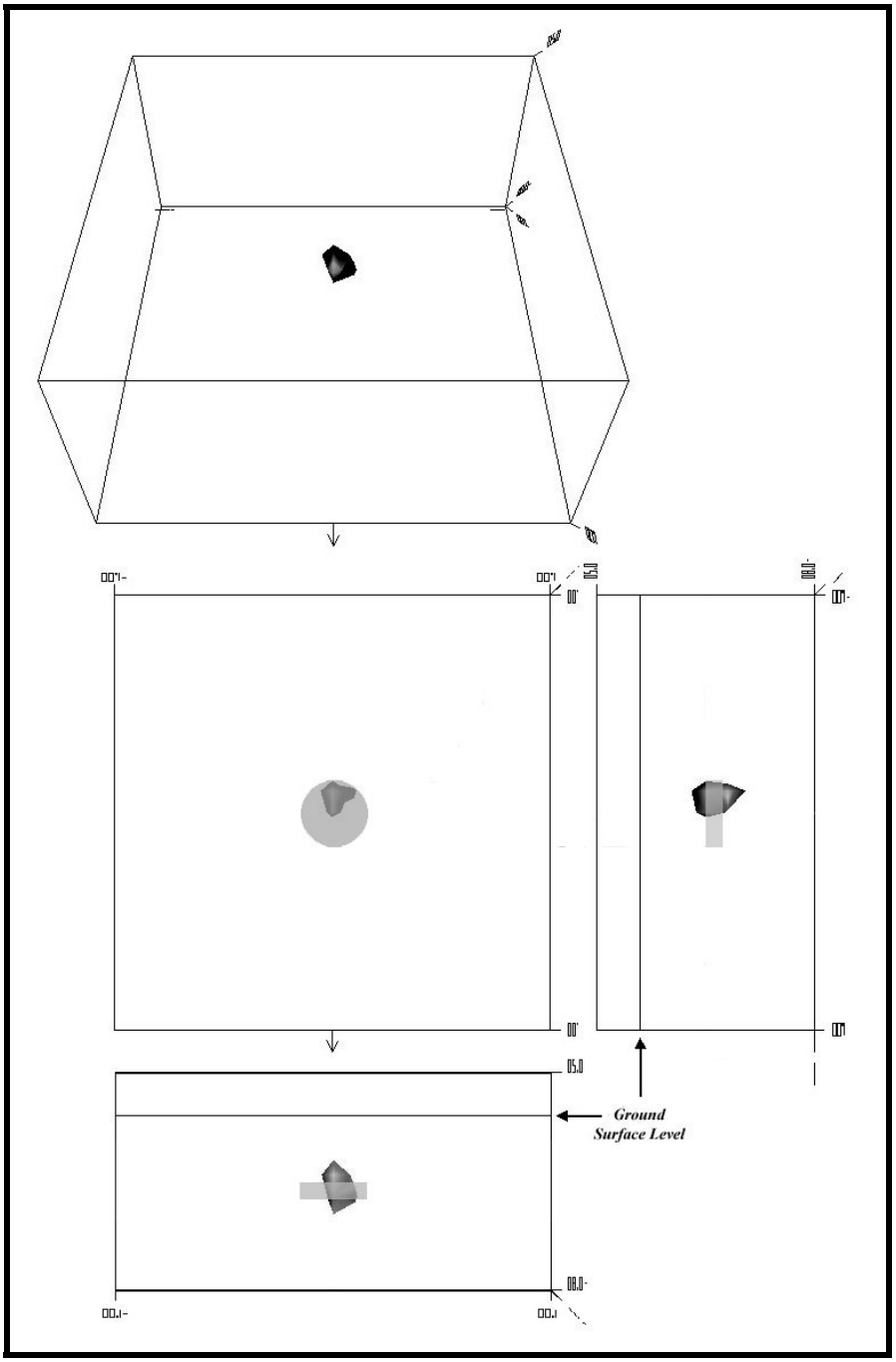

Figure 26 – Close-up SAR Image of Target T8 Buried 30 cm below the Surface With T8 Ground Truth Superimposed In Sectional Views. Volume Shown is 2 m x 2 m x 1 m.

Figure 27 is a 3D SAR image of target T7, the MK II grenade, on the surface. This was the smallest target tested. The volume shown is a cube having 1 m on a side. The vertical scale (z-dimension) is from +0.2 m above the surface to -0.8 m below the surface. The position of the ground surface level is shown in the front and side sectional views. For this particular image only a subset of the radar frequencies were used to produce the SAR image. Specifically, radar frequencies between 650 MHz and 1000 MHz were used in forming the SAR image (frequency data between 300 MHz and 1000 MHz were collected). The reason only the higher frequencies were used was because the target was small enough such that the longer radar wavelengths did not significantly contribute to target scattering but just added clutter. The reduced bandwidth of the image resulted in less resolution downrange (i.e., z-direction) contributing to the elongation of the SAR image in the z-direction.

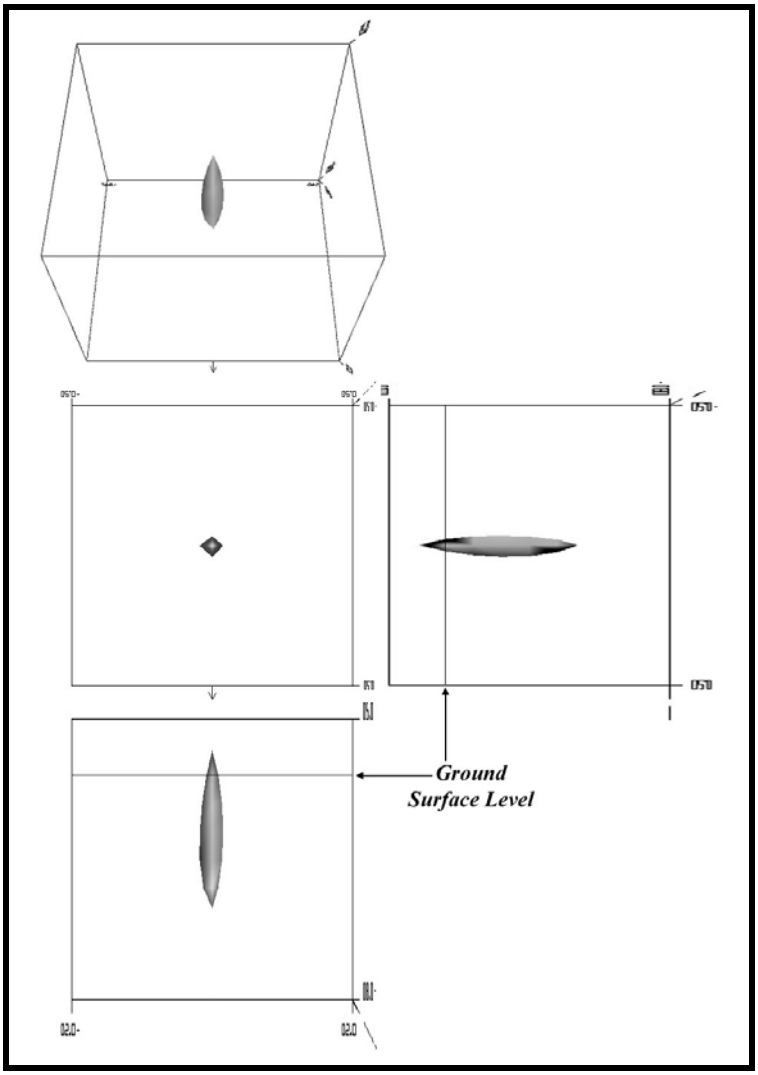

Figure 27 – Close-up SAR Image of Target T7, MKII Grenade, On the Surface. Volume Shown is 1 m x 1 m x 1 m. Limited BW of the Image Contributes To Image Elongation In the Z - Direction.

Matched Filter Results

SAR processing was performed on all data sets having good quality position data. For every data set processing was performed with and without matched filtering. The results of the processing comparison are presented in Table 6. The Matched Filter Benefit column is the difference between the processing gain achieved with and without matched filtering. Generally, a 3 dB gain or better is considered adequate to discriminate a target type.

TABLE 6 – Results of Matched Filter Processing Analysis

Target	Burial Depth	Matched Filter Benefit
T1	Surface	5.8
T1	30 cm	None
T2	Surface	3.8
T2	30 cm	BAD Data
T3	Surface	None
T3	30 cm	BAD Data
T4	Surface	1.4
T4	20 cm	BAD Data
T5	Surface	.6
T5	20 cm	BAD Data
T6	Surface	BAD Data
T6	20 cm	BAD Data
T7	Surface	.6
T7	10 cm	BAD Data
T8	Surface	.8
T8	20 cm	None
	Depth Is Surface to Target Center	Increased Processing Gain (dB)

5. Discussion of Results

The results of the testing and matched filtering processing were mixed. On the positive side, the standoff GPR sensor performed very well as far as the detection of surface and buried UXO targets. Additionally, the matched filter processing gains achieved for some of the UXO targets placed on the surface were significant enough to achieve some degree of target discrimination. However, the matched filter processing gains for all buried targets were negligible and, thus, were not particularly well suited for target discrimination purposes. These results were in contrast to the matched filter simulation model, which indicated that high processing gains could be achieved for buried targets.

This discrepancy between the simulation results and the actual data processing results most likely results from basic limitations associated with the computer model that underlies the matched filter SAR processing. Specifically, the model used is based on the physical optics approximation that essentially assumes propagation between the radar and

a buried target occurs as plane wave propagation. In fact, a physics-based model that better accounts for propagation associated with resonant regime physics may be required to realize potential processing gains as predicted by the simulations.

viii. Conclusions and Recommendations

The standoff GPR sensor that was tested was able to detect a variety of surface and buried UXO ranging in size from small (MK II grenade) to moderately sized (105 mm shell) targets. Furthermore, the matched filter processing technique was able to achieve significant processing gain for certain surface targets indicating the potential for discriminating UXO targets on the surface. However, the matched filter processing, as currently implemented, was unsuccessful in achieving any significant processing gains when used against buried targets resulting in negligible discrimination capability for this case. The discrepancy between the matched filter simulation modeling, which indicated a significant potential for discrimination, and the actual data for buried targets is attributable to limitations in the models underlying the matched filter SAR image formation algorithm.

It is recommended that the standoff GPR system as currently configured be further developed for use as a standoff detection sensor for buried UXO. Specifically, by improvements in the system's mobile would improve the productivity and efficiency of the data collection process and allow larger areas to be economically surveyed. Additionally, it is recommended that the SAR matched filter processing technique be improved by utilizing a more rigorous physics-based electromagnetic model to calculate the propagation characteristics for targets buried underground targets. Furthermore, it is recommended that the new discrimination algorithms be designed to specifically exploit the unique data characteristics (e.g., wide angular diversity) afforded by the 3D spotlight mode SAR data collection method.

ix. Appendix A – Technical Abstract

A technical presentation was given discussing this project at the "Partners in Environmental Technology" Technical Symposium and Workshop, Technical Session No. 3A. The symposium was held on November 28-30, 2000 at the Hyatt Regency Crystal City Hotel in Arlington, VA. The text of the published technical abstract is provided below.

SAR/GPR Matched Filter Processing for UXO Discrimination

GEORGE J. MOUSSALLY, PH.D.
Mirage Systems
1031 East Duane Avenue, Suite F
Sunnyvale, CA 94085-2626
(408) 524-7905
geojm@ieee.org

This presentation describes the status and results of a SERDP Seed Project involving research and development of a "matched filter processing" technique to improve discrimination of buried UXO targets detectable by an existing Ground Penetrating Radar (GPR). The "matched filter processing" technique attempts to exploit target specific radar scattering features by incorporating them directly into the imaging process, which uses Synthetic Aperture Radar (SAR) techniques. The processing technique is applied to actual SAR data collected at Yuma Proving Grounds (YPG) on buried UXO targets. The existing GPR used for the project is a mobile, standoff system (i.e., the GPR antenna is remote from the ground surface) that uses SAR techniques to form 3D imagery of the subsurface environment. A specific objective of the technique is to reduce the number of false positives typically encountered in the UXO cleanup process. The basic processing methodology will be described as will the GPR system and the test performed at YPG. The results of buried UXO target scattering models using the NEC4 electromagnetic modeling code will be presented. Examples of 3D SAR imagery generated using the processing method will be described and the results of using the processing technique to reduce false alarm rate will also be presented.